Environmental Science & Technology

ARTICLE

pubs.acs.org/est

Evaluating the Mixing of Organic Aerosol Components Using High-Resolution Aerosol Mass Spectrometry

Lea Hildebrandt,[†] Kaytlin M. Henry,[†] Jesse H. Kroll,[‡] Douglas R. Worsnop,[§,⊥] Spyros N. Pandis,[†,∥] and Neil M. Donahue[†,*]

[†]Center for Atmospheric Particle Studies, Carnegie Mellon University, Pittsburgh, PA, USA

[‡]Department of Civil and Environmental Engineering, Massachusetts Institute of Technology, Cambridge, MA, USA

[§]Aerodyne Research, Billerica, MA, USA

[⊥]Department of Physical Sciences, University of Helsinki, Helsinki, Finland

[∥]Institute of Chemical Engineering and High Temperature Chemical Processes (ICE-HT), Foundation of Research and Technology (FORTH), Patra, Greece

Supporting Information

ABSTRACT: According to the pseudo-ideal mixing assumption employed in practically all chemical transport models, organic aerosol components from different sources interact with each other in a single solution, independent of their composition. This critical assumption greatly affects modeled organic aerosol concentrations, but there is little direct experimental evidence to support it. A main experimental challenge is that organic aerosol components from different sources often look similar when analyzed with an aerosol mass spectrometer. We developed a new experimental method to overcome this challenge, using isotopically labeled compounds (^{13}C or D) and a high-resolution time-of-flight aerosol mass spectrometer (HR-ToF-AMS). We generated mixtures of secondary organic aerosol (SOA) from isotopically labeled toluene and from unlabeled α-pinene and used the HR-ToF-AMS data to separate these different SOA types. We evaluated their interaction by comparing the aerosol mass yields of toluene and α-pinene when the SOA was formed in these mixtures to their yields when the SOA was formed in isolation. At equilibrium, our results are consistent with pseudo-ideal mixing of anthropogenic and biogenic SOA components from these chemically dissimilar precursors.

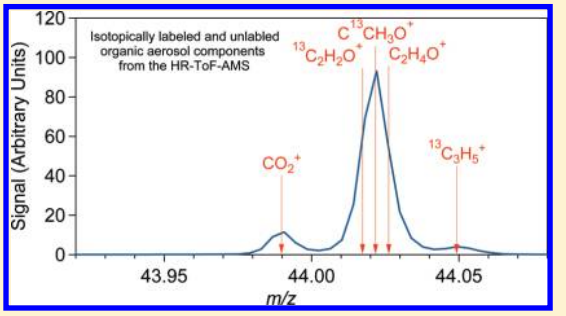

1. INTRODUCTION

Submicrometer atmospheric particles are of interest because they adversely affect human health[1] and because they have a highly uncertain effect on climate.[2] Organic aerosol (OA) globally comprises 20−90% of the submicrometer particle mass.[3] However, OA concentrations and characteristics calculated in chemical transport models (CTMs) often differ from ambient measurements of OA,[4,5] suggesting that the representation of OA in CTMs, which reflects our understanding, is incomplete and/or erroneous.

From a source perspective, OA can be classified as primary (POA) or secondary (SOA).[6] In this classification, POA refers to compounds that are emitted as particles. SOA is formed when volatile organic compounds (VOCs) undergo one or more chemical transformations in the gas phase, forming less volatile compounds that then partition to the particle phase. Most CTMs further distinguish between anthropogenic SOA (ASOA) and biogenic SOA (BSOA), formed from anthropogenic and biogenic VOCs, respectively.

The ability of a gaseous precursor to form SOA is usually described by a fractional aerosol mass yield − the mass of aerosol formed divided by the mass of VOC reacted. The initial formation of SOA is modeled as absorptive partitioning of semivolatile compounds between the gas and particle phases.[7−9] Most models assume that all organic species form a single, well-mixed organic phase that is able to absorb more organic vapors than if different OA species would form separate phases. This simplification was first suggested by Odum et al.,[8] who observed that the yield parameters derived from experiments using a single VOC could explain the total aerosol formation in experiments using two VOCs. Strader et al.[10] assumed that the Odum approach can be applied to OA from multiple sources by modeling OA as what they called a pseudo-ideal solution, incorporating any potential nonidealities in an effective saturation concentration of the organic species (the product of activity coefficient and saturation concentration), which is determined in laboratory experiments.

The pseudo-ideal mixing assumption has since been used in numerous other modeling studies;[11,12] however, there is little

Received: March 11, 2011
Accepted: June 9, 2011
Revised: May 25, 2011
Published: July 07, 2011

direct experimental evidence to support it. A main experimental challenge is to distinguish different types and sources of OA. Studies by Odum et al.[8,13] indirectly showed that ASOA and BSOA and the ASOA from gasoline vapors form pseudo-ideal mixtures. However, more recent experiments by Song et al.[14] may suggest that POA does not form a single phase with SOA. Asa-Awuku et al.[15] studied particle size distributions of OA mixtures and found that SOA forms a single phase with diesel POA but not with a motor oil/diesel fuel mixture.

Recently, Dommen et al.[16] used isotopic labeling (^{13}C) to increase the distinguishability of different types of OA, and they investigated the aerosol mass yield of isoprene in the presence of α-pinene SOA. They used several methods to collect the OA and then determined the concentration of isoprene SOA offline using isotope ratio mass spectrometry.[16] Their measured aerosol mass yield was consistent with isoprene SOA and α-pinene SOA (two different types of BSOA) forming a single phase. Because of filter sampling artifacts, their study was limited to aerosol concentrations exceeding 10 $\mu g\ m^{-3}$. Another source of uncertainty in their study was the conversion from measured concentrations of organic carbon to organic mass.[16]

In this study, we used a high-resolution time-of-flight aerosol mass spectrometer (HR-ToF-AMS)[17] from Aerodyne Research, Inc., which measures organic aerosol online, avoiding the uncertainties associated with filter collection and analysis. We used isotopically labeled species (^{13}C and D) to increase the distinguishability of the organic fragments. Isotopic labeling increases the nominal m/z and the mass defect of a given fragment, separating the isotopically labeled fragments from unlabeled organic fragments at the same nominal m/z. The ability of the HR-ToF-AMS to distinguish between isotopically labeled and unlabeled organic fragments had not been investigated prior to this study. As such, an important part of this work was to develop the analysis method using the HR-ToF-AMS to separate isotopically labeled and unlabeled OA. The main scientific goal was to test the pseudo-ideal mixing assumption. We here test this assumption for mixtures of SOA formed from toluene and from α-pinene, chemically dissimilar ASOA and BSOA precursors.

2. MATERIALS AND METHODS

2.1. Environmental Chamber Experiments. Organic aerosol from isotopically labeled toluene and from unlabeled α-pinene was sequentially formed in the environmental chamber of Carnegie Mellon's Center for Atmospheric Particle Studies (CAPS). Many of the experimental procedures have been published previously.[18] Hydrogen peroxide (HOOH) was used as an OH source for toluene photo-oxidation, and as an OH-scavenger during α-pinene ozonolysis. Before initiating α-pinene SOA formation, 2-butanol was also injected as an additional OH scavenger. Two different types of isotopically labeled toluene were used (Figure S1 of the Supporting Information): ^{13}C-toluene (Cambridge Isotope Laboratories, 99%) in which all six ring carbons were ^{13}C-substituted, leaving the methyl carbon unsubstituted; and D-toluene (Cambridge Isotope Laboratories, 99.5%) in which all eight hydrogens were substituted with deuterium. Concentrations of the VOCs were monitored using a proton-transfer reaction mass spectrometer (PTR-MS, Ionicon Analytik GmbH). Ozone (O_3) was produced from the HO_x + NO_x reactions during toluene photo-oxidation or it was generated using a commercial corona-discharge ozone generator (Azco, HTU500AC) and introduced into the chamber. Inorganic ammonium sulfate ($(NH_4)_2SO_4$, Sigma Aldrich, 99.99%) seed particles were used in all experiments to provide surface area for the condensation of organic vapors.

During each experiment, the formation of toluene SOA commenced when toluene and OH (from the photolysis of HOOH) were in the chamber, starting the oxidation of toluene. The formation of α-pinene SOA commenced when both α-pinene and O_3 were in the chamber, starting ozonolysis of α-pinene. Particle number and volume inside of the chamber were measured using a scanning mobility particle sizer (SMPS, TSI classifier model 3080, CPC model 3772 or 3010). Particle mass was measured by a HR-ToF-AMS.[17] The HR-ToF-AMS has two ion optical modes named by the shape of the ion flight paths: a single-reflection mode (V-mode) with a smaller flight path and hence higher sensitivity but lower resolution, and a double-reflection mode (W-mode) with longer flight path and hence higher resolution but lower sensitivity. We operated the HR-ToF-AMS according to the common protocol with the vaporizer temperature at 600 °C, alternating between V and W modes to collect mass spectra and particle time-of-flight (pToF) measurements in V-mode. Additional experimental details are provided in section S1 of the Supporting Information, and experimental conditions are summarized in Table S1 of the Supporting Information.

We present results from two main types of experiments forming α-pinene SOA in the presence of toluene SOA (experiments 1 and 2) and forming toluene SOA in the presence of α-pinene SOA (experiments 3 and 4).

2.2. HR-ToF-AMS Data Analysis. The HR-ToF-AMS data were processed in *Igor Pro 6.12* (Wavemetrics, Inc.) using the standard HR-ToF-AMS data analysis toolkits Squirrel version 1.48 and Pika version 1.08 (http://cires.colorado.edu/jimenez-group/wiki/index.php/ToF-AMS_Analysis_Software). Squirrel is used to determine the OA mass spectra at unit mass resolution (UMR analysis) and Pika is used to determine the OA mass spectra at high resolution by integrating individual ion peaks in the raw spectra (HR analysis). Total mass concentrations can be derived from UMR analysis and from HR analysis. Details on the AMS data processing are provided in section S2 of the Supporting Information.

2.2.1. Separation of Isotopically Labeled and Nonlabeled OA. We tested two different methods to separate the isotopically labeled and unlabeled HR organic mass spectra. The first method (direct method) uses the sum of the signal from labeled HR ions (minus the isotopically constrained contributions) and the sum of the signal from unlabeled HR ions and assumes that they correspond to the labeled OA and the unlabeled OA, respectively. Labeled HR ions are those containing D or ^{13}C; unlabeled HR ions contain only H and ^{12}C. The second method uses a chemical mass balance (CMB) approach,[19,20] separating the HR OA spectra by using the known spectra of the different types of OA (e.g., the ^{13}C-toluene SOA spectrum and the α-pinene SOA spectrum) and reconstructing the observed, mixed organic mass spectrum as a linear combination of the two known mass spectra. One concern with the D-toluene precursor is the possibility of hydrogen-shift reactions, which could confound the labeled/unlabeled distinction of the different OA types. We found evidence for the occurrence of hydrogen-shift reactions, but we are still able to attribute the ions to one of the precursors, as explained in more detail in section S3 of the Supporting Information. A difficulty with the ^{13}C-toluene precursor is the unlabeled methyl group ($^{12}CH_3$), which can result in unlabeled

HR ions from that precursor. A final challenge in separating the different types of OA stems from overlapping peaks, which can result in covariance of the recovered HR-ion signals, as discussed in detail in section S3 of the Supporting Information. In summary, we find that there is some covariance of integrated signals due to overlapping peaks, which presents a challenge to the direct method (Figure S3 of the Supporting Information). The covariance of overlapping peaks is accounted for in CMB because it uses the measured HR mass spectra of the isotopically labeled and unlabeled OA. We therefore used CMB for our final analysis.

We find the mass spectra of the different OA types from periods of the experiment when only one OA type was present. Because we formed the different types of OA sequentially in these experiments, we can only obtain the mass spectrum of the first OA type in each experiment and obtain the mass spectrum of the other OA type from a different experiment. For the CMB analysis of experiments 1 and 2, we used the α-pinene SOA spectrum from experiment 3; for the CMB analysis of experiments 3 and 4 we used the toluene SOA spectrum from experiment 1. We weighted all mass fragments equally in the CMB analysis and used a sensitivity analysis (section S4 of the Supporting Information) to quantify the overall uncertainty. The distinguishability of the OA mass spectra, which is important for our ability to separate them, is evaluated and discussed in section S5 of the Supporting Information.

2.2.2. Quantification of Organic Aerosol Production. We want to determine the aerosol mass yield, *Y*, defined as the ratio of the concentration of organic aerosol formed, divided by the mass of VOC reacted. Obtaining accurate measures of the total organic aerosol concentration C_{OA} is crucial for obtaining accurate aerosol mass yields. Details on the quantification of suspended organic aerosol concentrations C_{OA}^{sus} from the HR-ToF-AMS are presented in section S6 of the Supporting Information. To correct the total OA concentration for losses of particles and vapors to the chamber walls, we developed a general algorithm that does not rely on the OA/Sulfate ratio as in our previous study[18] and can therefore be used for both seeded and nucleation experiments. The mass balances of the organic aerosol in suspension C_{OA}^{sus} and the organic aerosol on the walls, C_{OA}^{wall}, are given by

$$\frac{d}{dt}[C_{OA}^{sus}(t)] = -k_{OA}^{w}(t)C_{OA}^{sus}(t) + P^{sus}(t) \quad (1a)$$

$$\frac{d}{dt}[C_{OA}^{walls}(t)] = k_{OA}^{w}(t)C_{OA}^{sus}(t) + P^{walls}(t) \quad (1b)$$

where $k_{OA}^{w}(t)C_{OA}^{sus}(t)$ is the loss rate of OA mass to the chamber walls due to deposition and P^{sus} and P^{walls} are the net rates of mass transfer of organic vapors to the particles in suspension and the particles on the walls, respectively. The wall deposition constant of organic aerosol $k_{OA}^{w}(t)$ can be estimated semiempirically by fitting the observed wall loss at times in the experiment when no OA is produced.[18] We want to find the total OA in the system, that is $C_{OA} = C_{OA}^{sus} + C_{OA}^{walls}$. The major unknown in the system of equations above is P^{walls}, which we cannot measure. We assume that the production of OA on the walls and in suspension is related by

$$\frac{P^{walls}(t)}{P^{sus}(t)} = w(t)\frac{C_{OA}^{walls}(t)}{C_{OA}^{sus}(t)} \quad (2)$$

where $w(t)$ is a proportionality coefficient. What we assume about $w(t)$ is of central importance. Most previous studies have neglected the condensation of organic vapors onto the wall-deposited particles ($w = 0$), however more recent data are consistent with $w = 1$.[18,21] The true value of w may lie somewhere in between these values. The parameter $w(t)$ could also depend on time; however, our understanding of the processes governing the condensation of organic vapors on the wall-deposited particles is currently insufficient to speculate about this, so we use constant w for the experiments presented here. We use $w = 1$ for toluene SOA production consistent with previous studies[18] and $w = 0$ for α-pinene SOA production, consistent with previous studies.[22]

The method we have suggested previously, calculating the total OA formed using the OA/sulfate, can be applied only in the case of $w = 1$ and when the wall-loss rates of OA and inorganic seed particles are equal. The algorithm we suggest here is more general and can be applied for any $w(t)$ and for any measured OA wall-loss rate. eq 2 assumes that organic vapors condense only onto wall-deposited OA and not onto the clean Teflon walls of the chamber, consistent with previous work.[18,21] Even though recent experimental evidence suggests that organic vapors may be lost to the Teflon walls,[23] these losses can currently not be measured or even estimated, so we do not consider them for this analysis.

Rearranging eq 1a and substituting into eq 2 we obtain:

$$P^{walls}(t) = w(t)\left(k_{OA}^{w}(t)C_{OA}^{sus}(t) + \frac{d}{dt}[C_{OA}^{sus}(t)]\right)\frac{C_{OA}^{walls}(t)}{C_{OA}^{sus}(t)} \quad (3)$$

We fit piecewise polynomials to the measured C_{OA}^{sus} (corrected as explained in section S6 of the Supporting Information) to be able to differentiate it easily. Substituting eq 3 into eq 1b:

$$\frac{d}{dt}[C_{OA}^{walls}(t)] = k_{OA}^{w}(t)C_{OA}^{sus}(t) + w(t)\left(k_{OA}^{w}(t)C_{OA}^{sus}(t) + \frac{d}{dt}[C_{OA}^{sus}(t)]\right)\frac{C_{OA}^{walls}(t)}{C_{OA}^{sus}(t)} \quad (4)$$

k_{OA}^{w} could theoretically change with time, but we assume here that it does not. We can measure k_{seed}^{w} (the rate constant for the wall loss of inorganic seeds) throughout the experiment since depositional wall loss is the only process affecting the inorganic seed concentration during the experiment. We here use $k_{OA}^{w} = k_{seed}^{w}$ since we have much more data to determine k_{seed}^{w} and we therefore deem it more accurate. The k_{OA}^{w} measured when OA was not forming was not significantly different from k_{seed}^{w}, consistent with an internal mixture.

The experiments presented here have the additional complication that two different types of OA are formed during the same experiment. The exact form of eq 4 then also depends on what we assume about the interaction of the different OA types. If we assume that the different OA types do not form a single solution we have two independent eqs 4 − one for toluene SOA and one for α-pinene SOA. If, however, we assume they form a single solution, the resulting ODEs are coupled:

$$\frac{d}{dt}[C_{TolOA}^{walls}(t)] = k_{OA}^{w}C_{TolOA}^{sus}(t) + w\left(k_{OA}^{w}C_{TolOA}^{sus}(t) + \frac{d}{dt}[C_{TolOA}^{sus}(t)]\right)\frac{C_{TolOA}^{walls}(t) + C_{ApOA}^{walls}(t)}{C_{TolOA}^{sus}(t) + C_{ApOA}^{sus}(t)} \quad (5a)$$

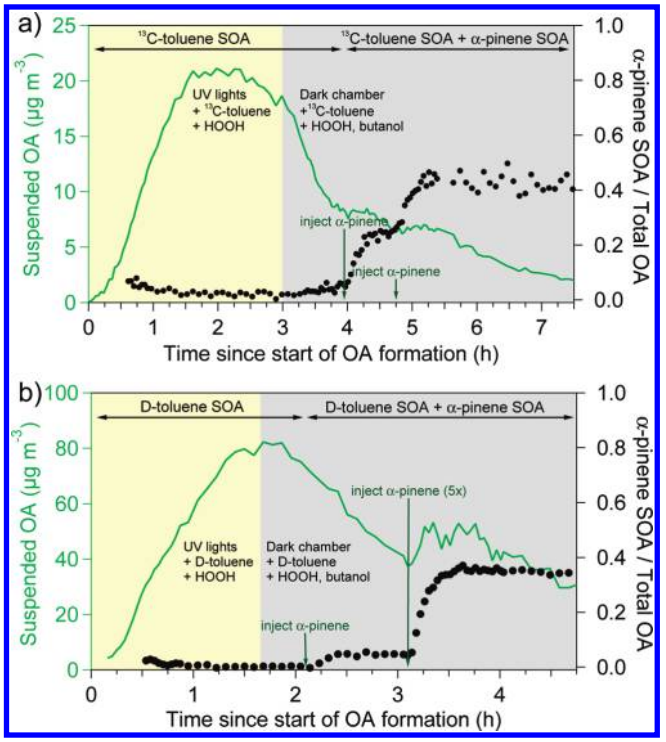

Figure 1. Time series of suspended OA concentrations (left vertical axis, green line, not corrected for wall losses) and the fraction of OA due to α-pinene SOA (right vertical axis, black circles) from the CMB analysis for experiments 1 (panel a) and 2 (panel b). The color of the background indicates different phases of the experiment with UV lights on (light yellow) and lights off (gray). In experiment 1, α-pinene SOA was formed in the presence of ^{13}C-toluene SOA seed; in experiment 2, α-pinene SOA was formed in the presence D-toluene SOA seed. The CMB results are consistent with the experimental sequences: the contribution of α-pinene SOA is practically zero before α-pinene is injected and increases after injection, leveling off after all of the α-pinene precursor (not shown) is consumed.

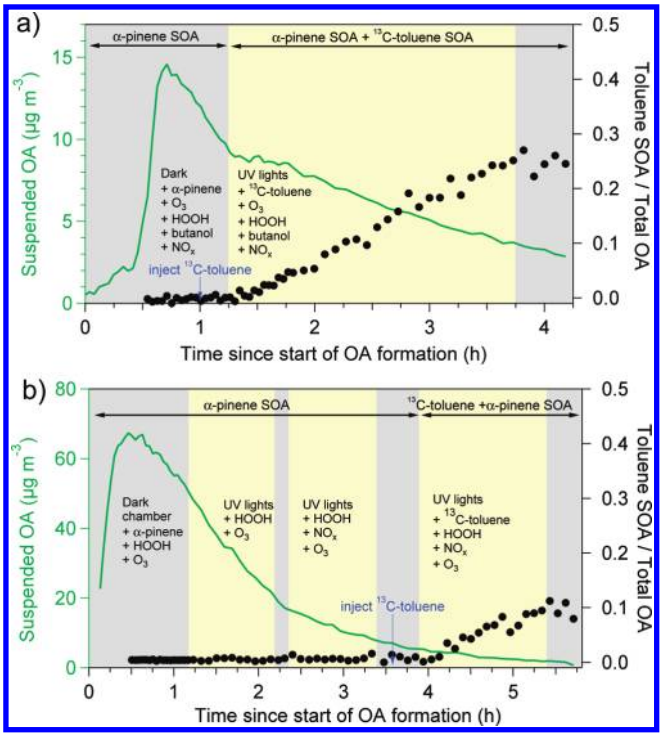

Figure 2. Time series of suspended OA concentrations (left vertical axis, green line, not corrected for wall losses) and the fraction of OA due to toluene SOA (right vertical axis, black circles) from the CMB analysis for experiment 3 (panel a) and experiment 4 (panel b). Time is referenced to the first O_3 injection (α-pinene was injected at $t < 0$). The color of the background indicates different phases of the experiment with UV lights on (light yellow) and lights off (gray). In both experiments, ^{13}C-toluene SOA was formed in the presence of α-pinene SOA. In experiment 4, α-pinene SOA was aged twice — first without and then with NO_x — before the formation of toluene SOA was started. The CMB results are consistent with the experimental sequences: the contribution of toluene SOA is practically zero until toluene is injected and UV lights are turned on, starting the formation of toluene SOA.

$$\frac{\mathrm{d}}{\mathrm{d}t}\left[C_{\mathrm{ApOA}}^{\mathrm{walls}}(t)\right] = k_{\mathrm{OA}}^{\mathrm{w}} C_{\mathrm{ApOA}}^{\mathrm{sus}}(t) + w\left(k_{\mathrm{OA}}^{\mathrm{w}} C_{\mathrm{ApOA}}^{\mathrm{sus}}(t) + \frac{\mathrm{d}}{\mathrm{d}t}\left[C_{\mathrm{ApOA}}^{\mathrm{sus}}(t)\right]\right)\frac{C_{\mathrm{TolOA}}^{\mathrm{walls}}(t) + C_{\mathrm{ApOA}}^{\mathrm{walls}}(t)}{C_{\mathrm{TolOA}}^{\mathrm{sus}}(t) + C_{\mathrm{ApOA}}^{\mathrm{sus}}(t)} \quad (5b)$$

Thus, to determine the organic aerosol concentration on the walls for the no mixing case, we solve eq 4 for toluene SOA and α-pinene SOA. For the ideal mixing case, we solve eqs (5). With the assumption of $w = 0$ for the formation of α-pinene SOA used in this work, eq 5b reduces to eq 4. Equations 4 and 5 are first-order differential equations in $k_{\mathrm{OA}}^{\mathrm{walls}}(t)$, which we solve numerically using a fifth-order Runge—Kutta—Fehlberg method. We can thus obtain $C_{\mathrm{OA}}^{\mathrm{walls}}(t)$ from eqs 4 or 5, $C_{\mathrm{OA}}^{\mathrm{sus}}$ from our measurements and can calculate the total OA in the system. Our analysis assumes that particles, specifically the toluene and α-pinene SOA, are internally mixed. This is consistent with HR-ToF-AMS data (Figure S4 of the Supporting Information), which show very similar size distributions of toluene SOA and α-pinene SOA.

We note that, even though this methodology for wall-loss correction is new, the specific cases investigated in this work ($w = 0$ and $w = 1$, $k_{\mathrm{OA}}^{\mathrm{w}} = k_{\mathrm{seed}}^{\mathrm{w}}$) are expected to yield the same results as methods used in previous studies. More specifically, the $w = 1$ case used in this work is similar to the OA/sulfate method we used previously,[18] and the $w = 0$ case used here is similar to previous methods that corrected the data only for the deposition of particles to the walls.[22] Advantages of this new method include that it allows for the testing of different assumptions about w and the extent of mixing, that it does not rely on the presence of inorganic seed aerosol, and that it makes the tracking of the two different OA types more straightforward.

3. RESULTS AND DISCUSSION

3.1. Separation of Different OA Types. Part a of Figure 1 shows time series from experiment 1 in which we first formed ^{13}C-toluene SOA and then α-pinene SOA. Ammonium sulfate seed particles, HOOH, and toluene were injected into the bag before the UV lights were turned on (time zero in Figure 1). Suspended organic aerosol concentrations (not corrected for wall losses, left vertical axis) increase during the first 1.5 h as ^{13}C-toluene is oxidized to form ^{13}C-toluene SOA; they decrease when wall losses start to dominate over the production of suspended OA. When α-pinene is injected, it is oxidized by O_3 to form α-pinene SOA. The production of α-pinene SOA is evident as bumps in the OA time series, but the OA increase is

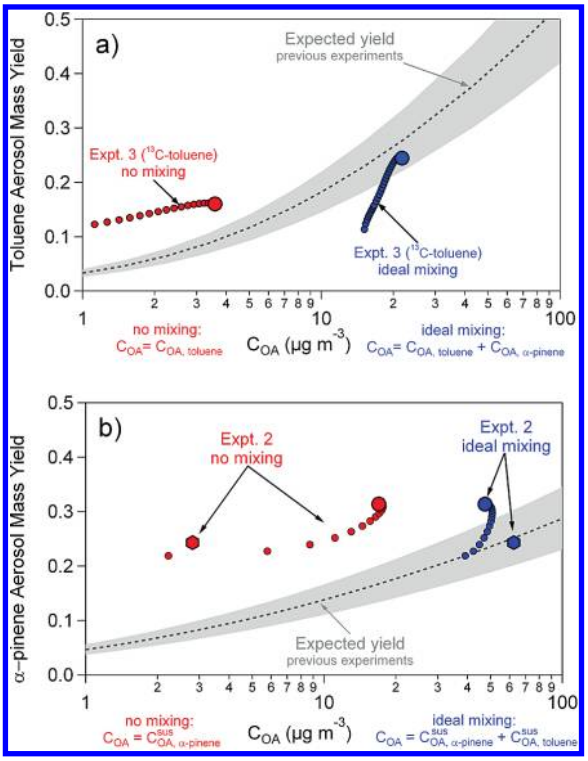

Figure 3. Evaluating the mixing behavior on standard yield plots for toluene SOA (panel a) and α-pinene SOA (panel b). For the no mixing case (red), SOA yields are plotted as a function of toluene SOA (a) or α-pinene SOA (b); for the ideal mixing case (blue), SOA yields are plotted as a function of total OA (α-pinene SOA + toluene SOA). The final yields (large symbols) are consistent with equilibrium partitioning. The two final yields in panel b each correspond to one α-pinene injection (first injection, hexagons). The dashed lines are yield fits based on previous experiments;[18,24] the shaded gray areas are ±20% of the yield fits, illustrating expected experimental variability.

confounded by OA decrease due to wall losses. The CMB results, however (right vertical axis), are clear and consistent with the experimental sequence: before α-pinene SOA formation, practically all OA is attributed to toluene SOA, and the fraction of α-pinene SOA to total OA is almost zero. When α-pinene is injected, the contribution of α-pinene SOA rises until all α-pinene (not shown) has reacted and then levels off.

The nonzero contribution attributed to α-pinene SOA by the CMB for $t < 1$ h could partially be due to OA contamination ($\sim$0.1 μg m^{-3} at $t = 0$), which is introduced when seed particles are injected. It could also be due to the low OA concentration at this time of the experiment because low signal increases uncertainty in the HR analysis. We tested the sensitivity of the CMB result to the inclusion of a contamination spectrum (section S4 of the Supporting Information) and found that it affects our final results by only 3−4%. Considering the OA contamination and low signal at the beginning of all experiments we do not include the CMB data for $t < 0.5$ h in Figures 1 and 2 for clarity.

Experiment 2 was analogous to experiment 1, but we used D-toluene SOA instead of ^{13}C-toluene SOA as an organic seed for α-pinene SOA formation. The separation of the different OA types by CMB was again successful (part b of Figure 1), in fact, the CMB result clearly showed α-pinene SOA formation after the first α-pinene injection, which was not visible in the suspended OA concentration. We injected about five times as much α-pinene in the second injection compared to the first which resulted in a correspondingly larger increase in the ratio of α-pinene SOA to total OA.

In experiments 3 and 4 (Figure 2), we used α-pinene SOA as a seed for ^{13}C-toluene SOA formation. The CMB results for experiment 3 (part a of Figure 2) are consistent with the experimental series: before the lights are turned on, no ^{13}C-toluene SOA is inside the bag and the ratio of ^{13}C-toluene SOA to total OA is zero. When the UV lights are turned on starting the photooxidation of toluene, the ratio of ^{13}C-toluene SOA to total OA increases steadily until the lights are turned off, after which it stays constant. In experiment 4, we turned on the UV lights twice before ^{13}C-toluene injection to age the α-pinene SOA with and without NO_x present in the chamber, thereby allowing us to explore how much the mass spectrum of α-pinene SOA changes with aging, and how much the aging of the mass spectrum may affect our CMB results. As part b of Figure 2 shows, CMB was again successful. Importantly, the separation of the two OA types was not affected greatly when we aged the OA: the contribution from ^{13}C-toluene SOA remained near-zero until toluene photooxidation was started. This observation, as well as our more quantitative analysis in sections S4 and S5 of the Supporting Information, suggests that changes in the mass spectra, which may result when UV lights are turned on in these experiments, do not affect the CMB results much.

Overall, we can conclude that the CMB analysis allows us to separate isotopically labeled organic aerosol (^{13}C or D) from unlabeled OA for all experiments conducted in this study. Thus, our new experimental method using isotopically labeled compounds and a HR-ToF-AMS to distinguish between different OA types is successful, and we can use the results to probe the pseudo-ideal mixing assumption for SOA from α-pinene and toluene.

3.2. Evaluation of Organic Aerosol Mixing. We evaluate the mixing behavior on standard yield plots for toluene (part a of Figure 3) and α-pinene (part b of Figure 3), which plot the aerosol mass yields as a function of the organic aerosol concentration. If the pseudo-ideal mixing assumption is valid and SOA from toluene and from α-pinene forms a single solution (the ideal-mixing case), the SOA yields of toluene should be a function of the total organic aerosol concentration in the system, and the SOA yields of α-pinene should be a function of the total suspended organic aerosol concentration, consistent with equilibrium partitioning. If, on the other hand, the SOA formed does not form a single solution with the pre-existing SOA (the no mixing case), the toluene SOA yields should be a function of only toluene SOA, and the α-pinene SOA yields should be a function of only the α-pinene SOA. The difference in the treatment of toluene and α-pinene SOA yields arises from different assumptions about the interaction of organic vapors with the walls ($w = 1$ and $w = 0$ for toluene and α-pinene SOA, respectively). The calculated toluene SOA yields are different for the two mixing cases due to the wall-loss correction, which depends on the mixing assumption (section 2.2.2).

The experiments presented here are especially sensitive to the interaction of organic vapors and the walls because the formation of the second SOA type commences a few hours into the experiment when often most of the SOA mass is on the walls. In experiments 1 and 2, the ratio of wall-deposited to suspended toluene SOA was 8.9 and 2.3 respectively when α-pinene SOA formation commenced. In experiments 3 and 4, the ratio of wall-deposited to suspended α-pinene SOA was 0.65 and 17

respectively when toluene SOA formation commenced. The calculated α-pinene SOA yields (experiments 1 and 2) and toluene SOA yields (experiments 3 and 4) are thus more uncertain in experiments 1 and 4 than in experiments 2 and 3. We therefore focus on the SOA yields from experiments 2 and 3 in the analysis below.

In part a of Figure 3, we plot the toluene aerosol mass yields from experiment 3, as well as a yield fit from our previous study.[18] We use results from experiment 3 to evaluate the pseudo-ideal mixing assumption by plotting the yields as a function of total OA and as a function of toluene SOA consistent with the ideal mixing and no mixing assumptions, respectively. Focusing first on the final yield (large symbols) we observe that the results are consistent with pseudo-ideal mixing (blue symbol falls into the expected range) and inconsistent with no mixing (red symbol falls outside of the expected range). The dynamic yields (small symbols) provide additional insights. First, the yields are clearly inconsistent with no mixing as they are much higher than expected from previous experiments. Second, the dynamic yields are consistent with mass-transfer limitations during organic aerosol formation because the yields early in the experiment are lower (the yield curves are steeper) than expected from previous experiments. There may be some delay between the condensation of organic vapors onto the pre-existing particles and the transfer of the organic species into the particle and equilibration with the bulk organic aerosol. Whereas our data are consistent with pseudo-ideal mixing at equilibrium, they do not rule out the possibility that these two different types of SOA form a partial mixture. The yield curve corresponding to an intermediate mixing case would fall in between the red and blue curves presented in part a of Figure 3 and would therefore be within the range of expected yields.

In part b of Figure 3, we plot the α-pinene aerosol mass yields from experiment 2, as well as a yield fit to previous studies using butanol as OH scavenger.[24] We use results from experiment 2 to evaluate the pseudo-ideal mixing assumption. There are two final yields, each corresponding to one α-pinene injection. We could not determine reliable dynamic yields for the first injection when α-pinene SOA formation was very fast. We note that the dynamic yields continue to increase when the suspended OA decreases due to wall loss (the yields curve to the left). This observation suggests that there is interaction of the α-pinene SOA vapors with the walls and that the $w = 0$ assumption may not be appropriate. However, using $w = 1$ results in yields exceeding 2, which is physically infeasible. Further understanding and constraining the interaction of organic vapors with the chamber wall is a topic of continued investigation. Overall, the α-pinene SOA yields are consistent with pseudo-ideal mixing and inconsistent with no mixing. The higher final yield from the second α-pinene injection (circle) could be associated with the use of HOOH as a second OH scavenger in these experiments, considering that recent studies have shown that yields from experiments using HOOH as OH scavenger are higher than those from experiments using butanol as OH scavenger.[24]

The calculated aerosol mass yields for experiments 1 and 4 are inconsistent (too high) with the ideal mixing and the no mixing cases. The agreement is better for the ideal mixing case (yields are about a factor of 2 higher than expected for both experiments) than for the no mixing case (yields are about a factor of 5 higher than expected for experiment 1 and at least a factor of 10 higher than expected for experiment 4). As mentioned before, this inconsistency is likely due to the uncertainties from the wall-loss correction, which are much larger in experiments 1 and 4 than in experiments 2 and 3 because the second reagent was added after a large fraction of the original SOA had deposited to the walls. This is a general challenge facing aerosol aging and mixing studies, where the required time delays force a buildup of material on chamber walls before the key part of an experiment begins.

In summary, we have developed a new method to separate different types of organic aerosol, using isotopically labeled precursors and a HR-ToF-AMS. Our results are consistent with mixing between SOA from toluene and α-pinene. The uncertainties associated with the nature of these experiments preclude us from ascertaining that the mixing between these different types of OA is ideal. Whereas our results are consistent with pseudo-ideal mixing, they would also be consistent with some intermediate extent of interaction. Nevertheless, our results suggest that ASOA and BSOA interact, and therefore that the presence of anthropogenic SOA enhances the concentrations of biogenic SOA, which has important implications for environmental policy.

■ ASSOCIATED CONTENT

Supporting Information. Details on experimental procedures and analysis methods are described as mentioned in the text. This material is available free of charge via the Internet at http://pubs.acs.org.

■ AUTHOR INFORMATION

Corresponding Author

*Phone: (412) 268-4415; Fax: (412) 268-7139; E-mail: nmd@andrew.cmu.edu.

■ ACKNOWLEDGMENT

This research was supported by the EPA STAR grant number R833746. This article has not been subject to EPA's required peer and policy review, and therefore does not necessarily reflect the views of the Agency. No official endorsement should be inferred. Lea Hildebrandt was supported by Graduate Research Fellowships from the National Science Foundation, the EPA STAR Program, the Teresa and H. John Heinz III Foundation, and John and Claire Bertucci.

■ REFERENCES

(1) Pope, C. A.; Dockery, D. W. Health effects of fine particulate air pollution: Lines that connect. *J. Air Waste Manage.* **2006**, *56*, 709–742.

(2) IPCC, Climate Change 2007 - The Physical Science Basis. *Contribution of Working Group I to the Fourth Assessment Report of the IPCC.* 2007.

(3) Zhang, Q.; Jimenez, J. L.; Canagaratna, M. R.; Allan, J. D.; Coe, H.; Ulbrich, I.; Alfarra, M. R.; Takami, A.; Middlebrook, A. M.; Sun, Y. L.; Dzepina, K.; Dunlea, E.; Docherty, K.; DeCarlo, P. F.; Salcedo, D.; Onasch, T.; Jayne, J. T.; Miyoshi, T.; Shimono, A.; Hatakeyama, S.; Takegawa, N.; Kondo, Y.; Schneider, J.; Drewnick, F.; Borrmann, S.; Weimer, S.; Demerjian, K.; Williams, P.; Bower, K.; Bahreini, R.; Cottrell, L.; Griffin, R. J.; Rautiainen, J.; Sun, J. Y.; Zhang, Y. M.; Worsnop, D. R., Ubiquity and dominance of oxygenated species in organic aerosols in anthropogenically-influenced Northern Hemisphere midlatitudes. *Geophys. Res. Lett.* **2007**, *34*; doi: 10.1029/2007gl029979.

(4) Karydis, V. A.; Tsimpidi, A. P.; Pandis, S. N., Evaluation of a three-dimensional chemical transport model (PMCAMx) in the eastern United States for all four seasons. *J. Geophys. Res.-Atmos.* **2007**, *112*; doi: 10.1029/2006JD007890.

(5) Volkamer, R.; Jimenez, J. L.; San Martini, F.; Dzepina, K.; Zhang, Q.; Salcedo, D.; Molina, L. T.; Worsnop, D. R.; Molina, M. J. Secondary organic aerosol formation from anthropogenic air pollution: Rapid and higher than expected. *Geophys. Res. Lett.* **2006**, *33*; doi: 10.1029/2006GL026899.

(6) Donahue, N. M.; Robinson, A. L.; Pandis, S. N. Atmospheric organic particulate matter: From smoke to secondary organic aerosol. *Atmos. Environ.* **2009**, *43*, 94–106.

(7) Donahue, N. M.; Robinson, A. L.; Stanier, C. O.; Pandis, S. N. Coupled partitioning, dilution, and chemical aging of semivolatile organics. *Environ. Sci. Technol.* **2006**, *40*, 2635–2643.

(8) Odum, J. R.; Hoffmann, T.; Bowman, F.; Collins, D.; Flagan, R. C.; Seinfeld, J. H. Gas/particle partitioning and secondary organic aerosol yields. *Environ. Sci. Technol.* **1996**, *30*, 2580–2585.

(9) Pankow, J. F. An absorption model of the gas/aerosol partitioning involved in the formation of secondary organic aerosol. *Atmos. Environ.* **1994**, *28*, 189–193.

(10) Strader, R.; Lurmann, F.; Pandis, S. N. Evaluation of secondary organic aerosol formation in winter. *Atmos. Environ.* **1999**, *33*, 4849–4863.

(11) Carlton, A. G.; Bhave, P. V.; Napelenok, S. L.; Edney, E. O.; G., S.; Pinder, R. W.; Pouliot, G. A.; Houyoux, M. Model representation of secondary organic aerosol in CMAQv4.7. *Environ. Sci. Technol.* **2010**, *44*, 8553–8560.

(12) Farina, S. C.; Adams, P. J.; Pandis, S. N., Modeling global secondary organic aerosol formation and processing with the volatility basis set: Implications for anthropogenic secondary organic aerosol. *J. Geophys. Res.* **2010**, *115*; doi: 10.1029/2009JD013046.

(13) Odum, J. R.; Jungkamp, T. P. W.; Griffin, R. J.; Flagan, R. C.; Seinfeld, J. H. The atmospheric aerosol-forming potential of whole gasoline vapor. *Science* **1997**, *276*, 96–99.

(14) Song, C.; Zaveri, R. A.; Alexander, M. L.; Thornton, J. A.; Madronich, S.; Ortega, J. V.; Zelenyuk, A.; Yu, X.-Y.; Laskin, A.; Maughan, D. Effect of hydrophobic primary organic aerosol on secondary organic aerosol formation from ozonolysis of α-pinene. *Geophys. Res. Lett.* **2007**, *34*; doi: 10.1029/2007GL030720.

(15) Asa-Awuku, A.; Miracolo, M. A.; Kroll, J. H.; Robinson, A. L.; Donahue, N. M. Mixing and phase partitioning of primary and secondary organic aerosols. *Geophys. Res. Lett.* **2009**, *36*; doi: 10.1029/2009GL039301.

(16) Dommen, J.; Hellen, H.; Saurer, M.; Jaeggi, M.; Siegwolf, R.; Metzger, A.; Duplissy, J.; Fierz, J.; Baltensperger, U. Determination of the aerosol yield of isoprene in the presence of an organic seed with carbon isotope analysis. *Environ. Sci. Technol.* **2009**, *43*, 6697–6702.

(17) DeCarlo, P. F.; Kimmel, J. R.; Trimborn, A. M.; Northway, M. J.; Jayne, J. T.; Aiken, A. C.; Gonin, M.; Fuhrer, K.; Horvath, T.; Docherty, K. S.; Worsnop, D. R.; Jimenez, J. L. Field-deployable, high-resolution, time-of-flight aerosol mass spectrometer. *Anal. Chem.* **2006**, *78*, 8281–8289.

(18) Hildebrandt, L.; Donahue, N. M.; Pandis, S. N. High formation of secondary organic aerosol from the photo-oxidation of toluene. *Atmos. Chem. Phys.* **2009**, *9*, 2973–2986.

(19) Miller, M. S.; Friedlander, S. K.; Hidy, G. M. A chemical element balance for the Pasadena aerosol. *J. Colloid Interface Sci.* **1972**, *39*, 165–176.

(20) Seinfeld, J. H.; Pandis, S. N. *Atmospheric Chemistry and Physics*, Second ed.; John Wiley & Sons: Hoboken, 2006.

(21) Weitkamp, E. A.; Sage, A. M.; Pierce, J. R.; Donahue, N. M.; Robinson, A. L. Organic aerosol formation from photochemical oxidation of diesel exhaust in a smog chamber. *Environ. Sci. Technol.* **2007**, *41*, 6969–6975.

(22) Presto, A. A.; Huff Hartz, K. E.; Donahue, N. M. Secondary organic aerosol production from terpene ozonolysis. 1. Effect of UV radiation. *Environ. Sci. Technol.* **2005**, *39*, 7036–7045.

(23) Loza, C. L.; Chan, A. W. H.; Galloway, M. M.; Keutsch, F. N.; Flagan, R. C.; Seinfeld, J. H. Characterization of vapor wall loss in laboratory chambers. *Environ. Sci. Technol.* **2010**, *44* (13), 5074–5078.

(24) Henry, K.; Donahue, N. M. Effect of the OH radical scavenger hydrogen peroxide on secondary organic aerosol formation from α-pinene ozonolysis. *Aerosol Sci. Technol.* **2011**, *45*, 686–690.